CONF-801091--7

MASTER

DISCLAIMER

This book was prepared as an account of work sponsored by an agency of the United States Government. Neither the United States Government nor any agency thereof, nor any of their employees, makes any warranty, express or implied, or assumes any legal liability or responsibility for the accuracy, completeness, or usefulness of any information, apparatus, product, or process disclosed, or represents that its use would not infringe privately owned rights. Reference herein to any specific commercial product, process, or service by trade name, trademark, manufacturer, or otherwise, does not necessarily constitute or imply its endorsement, recommendation, or favoring by the United States Government or any agency thereof. The views and opinions of authors expressed herein do not necessarily state or reflect those of the United States Government or any agency thereof.

THE NEED AND PROCEDURE FOR CALIBRATION OF FUEL ROD SIMULATORS*

NOTICE

PORTIONS OF THIS REPORT ARE ILLEGIBLE. It has been reproduced from the best available copy to permit the broadest possible availability.

R. D. Dabbs L. J. Ott
Engineering Technology Division
Oak Ridge National Laboratory
Oak Ridge, Tennessee 37830

ABSTRACT

Extensive experimental and analytical calibration procedures have been developed to fully classify fuel rod simulators (FRSs) in order to reduce the uncertainties in computed FRS surface temperatures and surface heat fluxes. Case studies are presented that show nonclassification of FRSs can result in severe errors in the calculation of the spatial and temporal history of the heat flow within the FRS as well as the surface heat flux and surface temperature.

INTRODUCTION

One of the primary objectives of the Oak Ridge National Laboratory (ORNL) Pressurized-Water Reactor Blowdown Heat Transfer (PWR-BDHT)

*Research sponsored by Division of Reactor Safety Research, U.S. Nuclear Regulatory Commission under Interagency Agreements DOE 40-551-75 and 40-552-75 with the U.S. Department of Energy under contract W-7405-eng-26 with the Union Carbide Corporation.

By acceptance of this article, the publisher or recipient acknowledges the U.S. Government's right to retain a nonexclusive, royalty-free license in and to any copyright covering the article.

DISTRIBUTION OF THIS DOCUMENT IS UNLIMITED

DISCLAIMER

This report was prepared as an account of work sponsored by an agency of the United States Government. Neither the United States Government nor any agency Thereof, nor any of their employees, makes any warranty, express or implied, or assumes any legal liability or responsibility for the accuracy, completeness, or usefulness of any information, apparatus, product, or process disclosed, or represents that its use would not infringe privately owned rights. Reference herein to any specific commercial product, process, or service by trade name, trademark, manufacturer, or otherwise does not necessarily constitute or imply its endorsement, recommendation, or favoring by the United States Government or any agency thereof. The views and opinions of authors expressed herein do not necessarily state or reflect those of the United States Government or any agency thereof.

DISCLAIMER

Portions of this document may be illegible in electronic image products. Images are produced from the best available original document.

Program [1] is the determination of fuel rod simulator (FRS) surface temperatures and surface heat fluxes from internal thermocouple responses during loss-of-coolant experiments (LOCE). This requires the solution of the inverse heat conduction problem [2].

The indirectly heated electric FRSs used in the BDHT bundle 1 (Fig. 1) had a dual-sheath design with thermocouples located in both the center of the FRS and in grooves in the outer surface of the inner sheath. These FRSs often had gaps between the inner and outer sheaths; furthermore, there was FRS-to-FRS variance in the manufacturing process, changes in bundle response due to aging, and considerable uncertainty in the thermal conductivity and thermal diffusivity of the electrical insulators [boron nitride (BN) and magnesium oxide (MgO)] used in the FRS construction. An extensive FRS calibration procedure (experimental and analytical) [3] was developed to supply FRS performance information to the inverse heat conduction model. These calibration procedures will briefly be reviewed and several case studies will be presented that illustrate that failure to fully classify FRSs with regard to component physical properties, gaps, etc. can result in severe errors during inverse calculations of the driving potential at the surface of the FRS (ΔT), the spatial and temporal history of the heat flow within the FRS, and the surface heat flux.

ROD CLASSIFICATION PROCEDURE

Experimental Procedure

Two types of experimental techniques can be used to generate the data required to classify the FRSs. Data from steady-state experiments

at varied power generation rates and FRS surface temperatures can be reduced to yield the desired gap information and the effective thermal conductivity of the BN annular insulator. Power drop tests ("controlled" transients) can be performed to determine the effective thermal diffusivity of the MgO core. It is assumed that centerline thermocouples exist in tandem with sheath thermocouples — that is, the rod centerline temperature *must* be monitored at the same axial position as that of the sheath thermocouple if the heater is to be fully classified. Without the centerline thermocouple, *only* the gap information can be extracted from calibration tests.

The fluid temperature (heat sink) range over which the experimental calibration runs can be made is largely dependent on the facility. As an upper limit for the sink temperature, (a function of the core flow rate, core inlet temperature, and pressure) the entire FRS should be maintained in the forced convection heat transfer regime. This conclusion is based on surface heat flux perturbation studies for the BDHT FRSs [4]. The lower limit of the heat sink temperature is also facility dependent {a function of the capability of the loop heat exchangers to remove the core and pump energy dissipated in the fluid or, in the case of the Thermal Hydraulic Test Facility (THTF), by the direct power current (whose magnetic field adversely affects thermocouple signals at low temperatures) supplied to the core [3]}.

Analytical Procedure

The result of the experimental FRS classification procedure is a magnetic tape generated by the THTF's computer operated data acquisition

system (CODAS) containing multiple steady-state and power drop information sets. These data sets are processed by a four-part calibration program, ORTCAL (ORNL Thermocouple Calibration).

ORTCAL — Part I

Part I of ORTCAL reads the steady-state calibration data sets (one at a time), computes the core coolant mass flow rate from a core heat balance, and calculates the local fluid conditions (i.e., bulk temperature, saturation temperature, and pressure) for each thermocouple level; subsequently, the heat transfer coefficient, heat transfer regime, FRS radial gap dimension, and FRS temperature profile are determined for each bundle thermocouple position. All of this information is accumulated, over the life of the bundle, on an ORTCAL thermocouple history tape.

The aging of THTF bundle 1 is illustrated in Fig. 2 for thermocouple position TE-318BG. This is a graph of the calculated gap width vs the number of times bundle 1 has been brought to power (with the curves drawn through approximately equivalent boundary conditions). Figure 2 shows gap closure when the FRS surface temperature is held constant and the FRS power-generation rate is increased (i.e., the inner sheath thermal expansion is greater than that of the outer sheath, thus closing the gap).

ORTCAL — Part II

Part II of ORTCAL uses temperatures indicated by the sheath and middle thermocouples along with the power generation rate to produce the effective thermal conductivity of the BN insulator. If the temperature

dependencies of the substrate thermal conductivities and the power generation rate are known, the FRS centerline temperature can be determined from the sheath thermocouple response independent of the core MgO thermal properties. It is assumed that the thermal conductivity of the BN can be approximated by a polynomial in terms of temperature, that is

$$k_{BN}(T) = C_1 + C_2T + C_3T^2 + C_4T^3 , \quad (1)$$

where C_i are the polynomial coefficients. Thus, given a set of coefficients C_i, the FRS centerline temperature (T_{center_j}) can be calculated for each steady-state observation j given the following boundary conditions for each observation: (1) the sheath thermocouple response and (2) the linear power-generation rate.

The regression procedure for determining the temperature dependence of k_{BN} [Eq. (1)] involves the minimization of the sum-of-squares function

$$F(C_1, C_2, C_3, C_4) = \sum_{j=1}^{N} (Y_{center_j} - T_{center_j})^2 \quad (2)$$

with respect to the C_i parameters, where Y_{center_j} represents the observed middle thermocouple response, T_{center_j} is the calculated steady-state FRS centerline temperature, and N is number of observations.

The technique employed for optimizing Eq. (2) is a numerical algorithm using a pattern search strategy.

~~The in situ correlation for thermocouple position TE-318BG and literature values for the thermal conductivity of annular BN are compared in Fig. 3.~~

ORTCAL — Part III

The thermal conductivity of MgO is a strong function of its packed density. Since the construction procedure for the THTF bundle 1 FRSs involves a series of swaging operations with certain axial sections of the FRS being swaged more than others, the estimated density of the MgO ceramic core ranges from 70 to 90% of the theoretical density.

Part III of ORTCAL uses the temperatures indicated by the sheath and the middle thermocouples along with the power generation rate to produce the effective thermal diffusivity of the MgO core, α_{MgO}. The thermal conductivity of the MgO is actually regressed upon as values for the density and specific heat of MgO are well defined. [The regressions of ORTCAL — Part II (determination of the effective thermal conductivity of the BN insulator) must precede the regressions of ORTCAL — Part III.]

Power drop tests (i.e., "controlled" transients) information is used by Part III of ORTCAL. These tests involve tripping the power to the bundle with the core mass flow rate and core inlet pressure and temperature remaining essentially constant throughout the test.

It is assumed that the thermal conductivity of MgO can be approximated by a polynomial in terms of temperature, that is

$$k_{MgO}(T) = C_1 + C_2T + C_3T^2 + C_4T^3 + C_5T^4 , \qquad (3)$$

where C_i are the polynomial coefficients. The MgO thermal diffusivity regression is based on minimization of the following sum-of-squares function,

$$F(C_1, C_2, C_3, C_4, C_5) = \sum_{j=1}^{N} \left[\sum_{i=1}^{\eta} (Y_{center_i} - T_{center_i})^2 \right]_j , \qquad (4)$$

with respect to the C_i parameters. The term Y_{center_i} represents the observed middle thermocouple response, T_{center_i} is the calculated FRS centerline temperature, η is the number of observations per power drop, and N is the total number of power drops.

Part III solves the forward conduction problem given a set of coefficients C_i and the following boundary conditions: (1) power generation rate as a function of time and (2) sheath thermocouple response as a function of time. Equation (4) is optimized by the same numerical pattern search technqiue used in Part II of ORTCAL.

~~A plot of the regression fits for TE-301DJ and TE-318BG vs literature data for the thermal conductivity of MgO is shown in Fig. 4.~~

ORTCAL — Part IV

Part IV of ORTCAL applies regression analysis to the results from Part I to determine the thermal expansion coefficients and proper bias points for the stainless steel annuli forming the gap. The mechanical model chosen to utilize this information is one dimensional, which is consistent with the thermal model used in the inverse calculation. The linear gap model used is

$$\Delta gap = \Delta gap_0 + \Delta\bar{r}_{NS} - \Delta\bar{r}_{NOD5} , \qquad (5)$$

where subscript 0 denotes the ~~bias~~ reference gap and subscripts NS and NOD5 refer to the first node in the outer sheath and the last node in the inner sheath, respectively. The values of $\Delta\bar{r}$ in Eq. (5) can be expanded ~~via the definition for the coefficient of linear expansion to yield~~ by the following equation, which was derived [2] from the definition for the coefficient of linear expansion:

$$L - L_0 = L_0 \{ \exp [C_1(T-T_0) + C_2(T^2-T_0^2) + C_3(T^3-T_0^3)] - 1.0 \} \qquad (6)$$

where L_0 and T_0 are the reference length and temperature respectively. Expanding $\Delta\bar{r}_{NS}$ and $\Delta\bar{r}_{NOD5}$ by using eq. (6) and inserting the expansion in eq. (5) yields

$$\Delta gap = \Delta gap_0 + \bar{r}_{NS} \{\exp[C_1(T_{NS} - T_{NS|_0}) + C_2 (T_{NS}^2 - T_{NS|_0}^2) + C_3(T_{NS}^3 - T_{NS|_0}^3)] - 1.0\} - \bar{r}_{NOD5} \{\exp[C_1(T_{NOD5} - T_{NOD5|_0}) + C_2(T_{NOD5}^2 - T_{NOD5|_0}^2) + C_3(T_{NOD5}^3 - T_{NOD5|_0}^3)] - 1.0\} . \quad (6)$$

The term Δgap_0 is the ~~bias~~ reference gap and $T_{NS|_0}$ and $T_{NOD5|_0}$ are the ~~bias~~ reference nodal temperatures.

Since the gap behavior can be expressed in one concise mathematical formula [Eq. (6)], a nonlinear least-squares routine (rather than the pattern search technique used previously) is employed to determine the coefficients C_i in Eq. (6).

CONSEQUENCES OF NONCALIBRATION OF FUEL PIN SIMULATORS

The effect of not classifying FRSs can best be illustrated by a series of examples that consist of ORINC [2] calculations for on THTF test 105, where the annular BN thermal conductivity, core MgO thermal diffusivity, and gap between the sheaths were varied to qualitatively assess their effect on the inverse calculations. At present, the only alternative to the calibration procedures just developed is to use literature data for the BN and MgO thermal conductivities and to assume that there is no gap between the sheaths. Therefore, ORINC case studies were made using the following combinations:

1. Case 1. ORTCAL regressions for BN thermal conductivity and MgO thermal diffusivity and the sheath-gap model;
2. Case 2. ORTCAL regression for k_{BN} and α_{MgO} and all gaps zeroed;

3. Case 3. Least-squares fits to literature data for k_{BN} and α_{MgO} and ORTCAL regressions for the sheath-gap model;

4. Case 4. Least-squares fits to literature data for k_{BN} and α_{MgO} and all gaps zeroed.

Case 1 will be used as the base case; case 4 is the current state-of-the-art practice.

Typical FRS surface temperature plots for case 1 at thermocouple level E are presented in Fig. 5.[3] Similar plots for the surface heat flux are given in Fig. 6.[4] The corresponding set of plots for case 2 is presented in Figs. 7[5] and 8.[6]

A comparison of Figs. 6[4] and 8[6] reveals little difference in the computed surface heat fluxes. This should be expected since the inverse solutions of the transient conduction equation for cases 1 and 2 will yield identical results for the computed temperature profile from the sheath thermocouple to the FRS centerline and for the heat flow through the sheath thermocouple. Thus, since the heat flow at the sheath thermocouple is the same for both cases, the temperatures in the outer stainless steel sheath must be higher for case 2 because the thermal resistance of the gap has been removed. Not only will the temperatures in the outer sheath be higher, the computed surface heat flux will also be slightly different because of the temperature dependence of the specific heat and thermal conductivity of stainless steel.

The noteworthy difference between cases 1 and 2 is obvious when Figs. 5[3] and 7[5] are compared; there is a significant discrepancy in the surface temperature plots in the pre- and post-critical heat flux (CHF) regions.

For case 1 at 0 s on level E, the FRS surface temperatures range from 601.7 to 605.9 K with a predicted heat transfer mode of forced convection; however, for case 2 (zero gaps), the heat transfer mode changed to nucleate boiling and the FRS surface temperature range became 621.8 to 674.4 K. There are similar results for 2 s into the transient, with an FRS surface temperature range of 773.2 to 796.4 K for case 1 and an FRS surface temperature range of 780.1 to 815.3 K for case 2. The calculated surface temperatures for case 2 are higher than those for case 1, and the range is much broader. The question of which case is more accurate must be answered because, as noted earlier, the calculated surface fluxes do not vary significantly between the two cases but the driving potential (i.e., $T_{surface} - T_{sink}$) is drastically different. As a result, the computed surface heat transfer coefficient would be greatly affected.

A study of the steady-state conditions (at 0 s) for cases 1 and 2 gives a reasonable answer to the above question. Case 1 predicts forced convection at level E. Using the Dittus-Boelter correlation, a heat transfer coefficient of 3.6×10^4 W/(m^2·K) is predicted at this level. The mean of the coefficients determined by ORINC for level E in case 1 is 3.77×10^4 W/m^2·K (17 observations with a standard deviation about the mean of 0.05×10^4 W/m^2·K). At steady-state, the mean surface heat flux for level E is 1.290×10^6 W/m^2 (17 observations with a standard deviation about the mean of 0.020×10^6 W/m^2). If the surface temperature for level E is calculated by

$$T_{surf} = T_{bulk} + \frac{\bar{\phi} \pm 3\delta_{\bar{\phi}}}{h_{D-B}} , \qquad (7)$$

the expected surface temperature range for level E would be 604.2 to 607.5 K, essentially the range determined for case 1. In case 2, for the nucleate boiling regime to be chosen by ORINC, the FRS model had to transfer heat to a sink temperature equal to the saturation temperature (619.0 K at 15709.2 kPa). If Thom's correlation is used for the subcooled nucleate boiling regime, the expected surface temperature range for level E can be determined by

$$T_{surf} = T_{sat} + 0.0406\ (\bar{\phi} \pm 3\delta_{\bar{\phi}})^{1/2}\ e^{-P/8687} . \qquad (8)$$

The expected range for level E would be 626.4 to 626.7 K if the local fluid pressure is used; however, the computed surface temperature range is 621.8 to 674.4 K. If there are pressure fluctuations radially at level E, the local pressures required to produce the computed rod surface temperatures for case 2 must be determined. Assuming Thom's correlation is applicable and using the rod surface heat fluxes (at 0 s), the local pressures shown in Fig. 9 would be required. From Fig. 9, it should be readily apparent that the existence of such radial pressure differences at one axial level in the core is physically impossible. Thus, it can be concluded that case 1 describes the surface conditions at level E best and that case 2 (with the zero gap assumption) grossly miscalculates the surface temperatures.

Case 3 of the study was an attempt to determine *only* the effect on the inverse calculations of using literature data for the insulator thermal conductivities; thus, both cases 1 and 3 use the ORTCAL dynamic gap model and gap regressions. The only differences between cases 1 and 3 are

the regression fits for k_{BN} and α_{MgO}. Fits to the literature data yield *higher* thermal conductivities values for both BN and MgO than those predicted by the ORTCAL regressions. The ORINC results at thermocouple position TE-318BG for THTF test 105 will be reviewed for cases 1 and 3.

A case result will be defined to be correct if the calculated FRS internal thermal response from ORINC matches or closely approximates the actual internal response from an FRS centerline thermocouple. The centerline thermocouple provides the means for independent verification of the model results.

The ORINC-calculated surface heat fluxes for cases 1 and 3 (case 4 is also included) are overlaid in Fig. 8 for the first 18 s of the transient, with the corresponding surface temperatures presented in Fig. 9. There appear to be minimal differences between cases 1 and 3; however, there is a very deceiving compression effect from the ordinate scale factor (this will be reviewed later). Figure 10 is an overlay of the ORINC calculated FRS centerline temperature response for cases 1 and 3 (case 4 is also included) with the response from thermocouple TE-318MG (the centerline thermocouple relative to TE-318BG). Note that case 1 very closely approximates the response of TE-318MG; however, case 3 not only initializes incorrectly at steady state but responds too fast, peaks too high, and rolls off too fast.

The incorrect setup in steady state for case 3 (the centerline temperature is ~18 K low) is caused solely by the BN thermal conductivity. As stated earlier, a fit to literature data for the thermal conductivity of BN yields higher values than those predicted by the ORTCAL regressions; therefore, for the same power-generation rate, less thermal gradient is

required in case 3 to move the heat through the BN and thus the centerline temperature is lower. As a result of the lower temperature profile, the total heat content of the FRS is less at steady state. A comparison of the overall heat balance for cases 1 and 3 shows that the total heat removed per unit length of FRS, Q', as defined by

$$Q' = 2\pi r_{surf} \int_0^{t_{end}} \phi_{surf}\, dt \,, \qquad (9)^{10}$$

where

ϕ_{surf} = surface heat flux,

r_{surf} = outside FRS radius,

t_{end} = total transient duration,

is 1.8% less for case 3 [43.843 (W·h)/m for case 1]. The total energy supplied to the FRS is the same for both cases [39.944 (W·h)/m], but the change in internal energy for case 3 is ~20.3% less than that for case 1 [3.957 (W·h)/m for case 1]. Since the final temperature profile for cases 1 and 3 is essentially the same (i.e., the final heat content of the FRS would be the same), the error is in the steady-state initialization.

The 1.8% difference between Q_1' and Q_3' is not distributed evenly over the time interval 0 to t_{end}. As noted earlier, Fig. ~~10~~ 8 is misleading due to the ordinate scaling.

The time range, 0 to 18 s, can be broken down into time intervals over which the value of the surface heat flux does not vary orders of magnitude. Over the time intervals of 0 to 0.65 and 3.3 to 18.0 s, the calculated surface heat flux and surface temperature for cases 1 and 3 are basically the same. The 3.3 to 18.0 s similarity is due to one of the primary forcing functions, the power generation rate, ramping to ~1/10 of

its steady-state value by 3.3 s and further ramping to 0.0 by 6.0 s. The 0.0 to 0.65 s similarity is due to the FRS at this position (TE-318BG) being in nucleate boiling in steady state and remaining so until CHF at ~0.5 s; thus, there is little change in the internal response until ~0.6 s. Over the 0.65- to 3.0-s interval, the calculated heat flux for case 3 ranges from 0.0 to 40.0% lower than for case 1. Figure ~~13~~ 11 gives a plot of the surface heat flux ratio (case 3/case 1) for the 0.50- to 3.40-s time interval. The general conclusion is that the inverse computed surface heat flux can be off by as much as 40% in comparing cases 3 and 1.

The general observation that the interior of the FRS responds too fast in case 3 is obvious in Fig. ~~12~~ 10. The FRS active component (Inconel-600) temperature (at r = 0.3 cm) is higher in case 1, eventually peaking at 2.15 s at 1061 K in case 1 and 1036 K in case 3, but the MgO temperatures (at r ≤ 0.2764 cm) being ~18 K lower at 0.0 s in case 3 actually become higher in case 3 as the transient progresses. Since the thermal diffusivity of the MgO is higher in case 3, the thermal resistance is less and thus more heat goes into the core of the FRS. Therefore, the centerline temperature in case 3 will respond faster and peak higher. The centerline temperature peaks at 1013 K at 3.20 s and at 996 K at 4.45 s for cases 3 and 1, respectively. The primary reason that the case 3 surface heat flux is less than that of case 1 in the 0.65- to 3.40-s time interval is that more heat is being driven into the interior of the FRS rather than to the surface.

Where neglect of the gap between the sheaths (as in case 2) affects the driving potential at the surface of the FRS, the use of literature

data for k_{BN} and α_{MgO} alters the spatial and temporal history of the heat flow within the FRS and, as a result, the computed surface heat flux.

Case 4 will not be discussed to any extent other than to say that it represents the superposition of the errors in cases 2 and 3 and the state-of-the-art thermal analysis of FRSs prior to ORTCAL and ORINC.

CONCLUSIONS

An experimental thermocouple calibration procedure and four-part calibration program, ORTCAL (ORNL Thermocouple Calibration), have been developed to supply FRS performance information to the inverse heat conduction model and program ORINC.

Case studies have shown that failure to fully classify FRSs with regard to component physical properties, gaps, etc. can result in severe errors during inverse calculations of the driving potential at the surface of the FRS (ΔT), the spatial and temporal history of the heat flow within the FRS, and the surface heat flux.

REFERENCES

1. *Project Description ORNL-PWR Blowdown Heat Transfer Separate-Effects Program — Thermal Hydraulic Test Facility (THTF),* ORNL/NUREG/TM-2 (February 1976).

2. L. J. Ott and R. A. Hedrick, *ORINC — A One-Dimensional Implicit Approach to the Inverse Heat Conduction Problem,* ORNL/NUREG-23 (November 1977).

3. L. J. Ott and R. A. Hedrick, *ORTCAL — A Code for THTF Heater Rod Thermocouple Calibration,* NUREG/CR-0342 (ORNL/NUREG-51) (February 1979).

4. L. J. Ott and K. W. Childs, *Surface Heat Flux Perturbations in BDHT Fuel Pin Simulators,* NUREG/CR-0610 (ORNL/NUREG-54) (April 1979).

5. J. E. Campbell and E. M. Sherwood, *High-Temperature Materials and Technology,* Wiley, New York.

6. C. D. Pears, Southern Research Inst., USAF ASD-TDR-62-765, 1-402 [AD 298-061].

7. V. Casal et al., KFK-2368, fur Kernforschung M.B.H. (September 1976).

8. Y. S. Touloukian, *Thermophysical Properties of High Temperature Solid Materials,* The Macmillan Company, New York, 1967.

BIOSKETCH

The authors are development engineers in the Analysis Group of the Oak Ridge National Laboratory (ORNL) Pressurized-Water Reactor Blowdown Heat Transfer (PWR-BDHT) Separate-Effects Program.

Mr. Dabbs is a 1977 nuclear engineering graduate of The University of Tennessee at Knoxville.

Mr. Ott is also a graduate of The University of Tennessee at Knoxville (1968, B.S. Chemical Engineering; 1978, M.S. Chemical Engineering).

ORNL-DWG 75-12382R

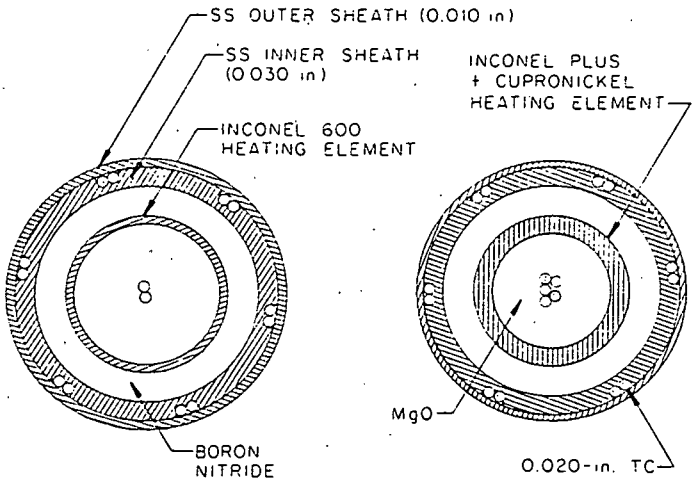

Fig. 1. Bundle 1 heater rod cross section (1 in. = 2.54 cm).

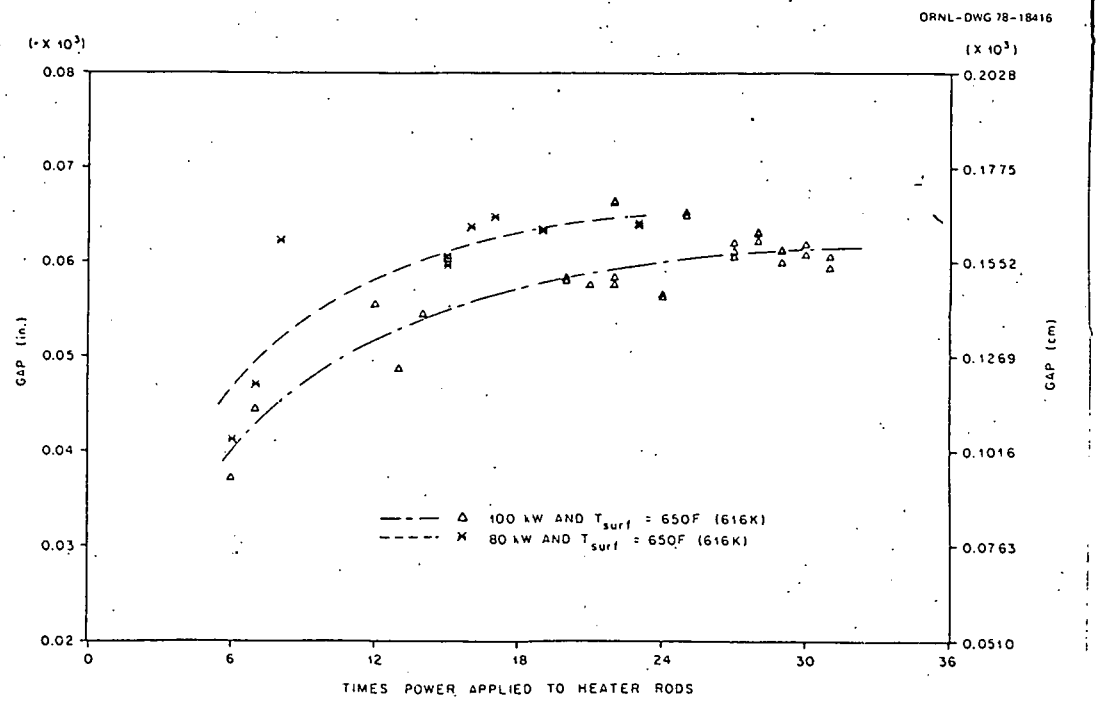

Fig. 2. Bundle 1 gap aging history at thermocouple position TE-318BG.

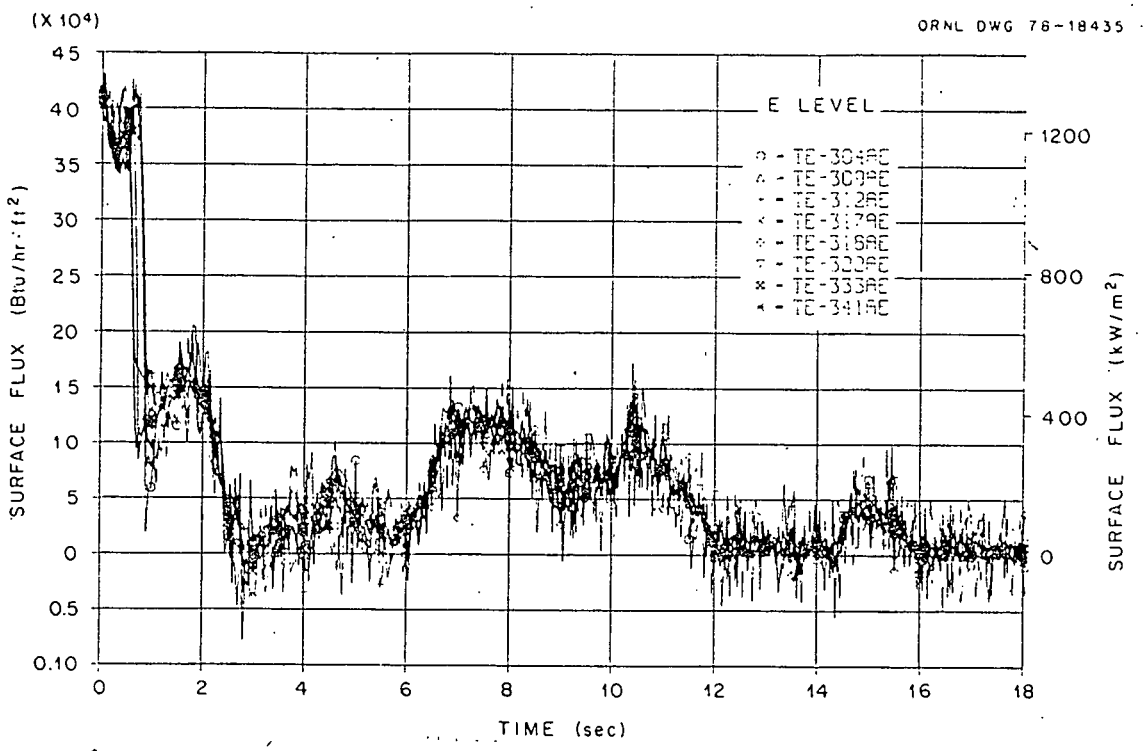

Fig. 5.4 ORINC calculated FRS surface heat fluxes, level E, THTF test 105, case 1.

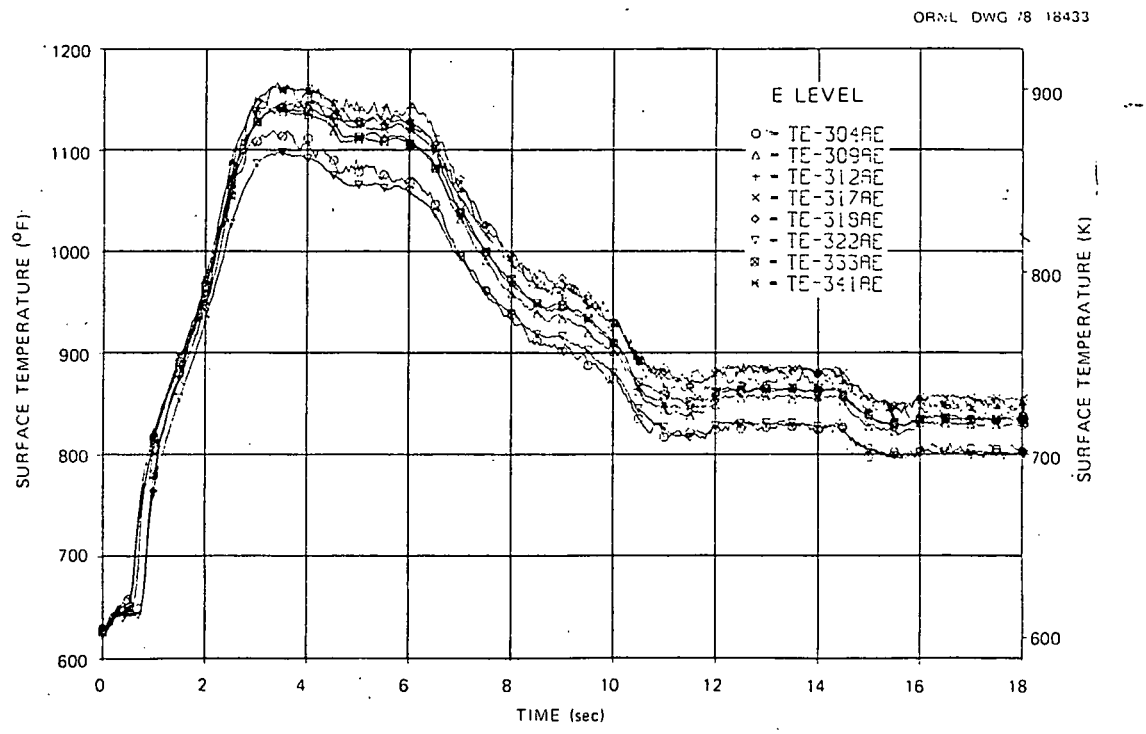

Fig. 5.3 ORINC calculated FRS surface temperatures, level E, THTF test 105, case 1.

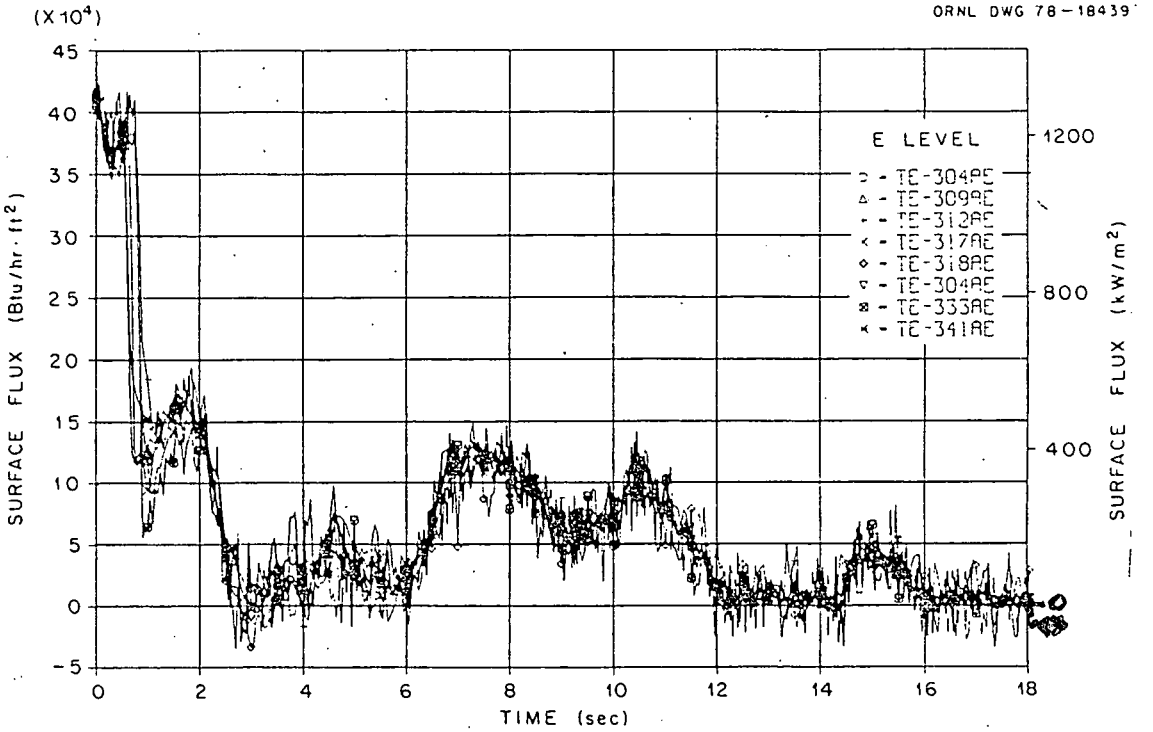

Fig. 8.6 ORINC calculated FRS surface heat fluxes, level E, THTF test 105, case 2.

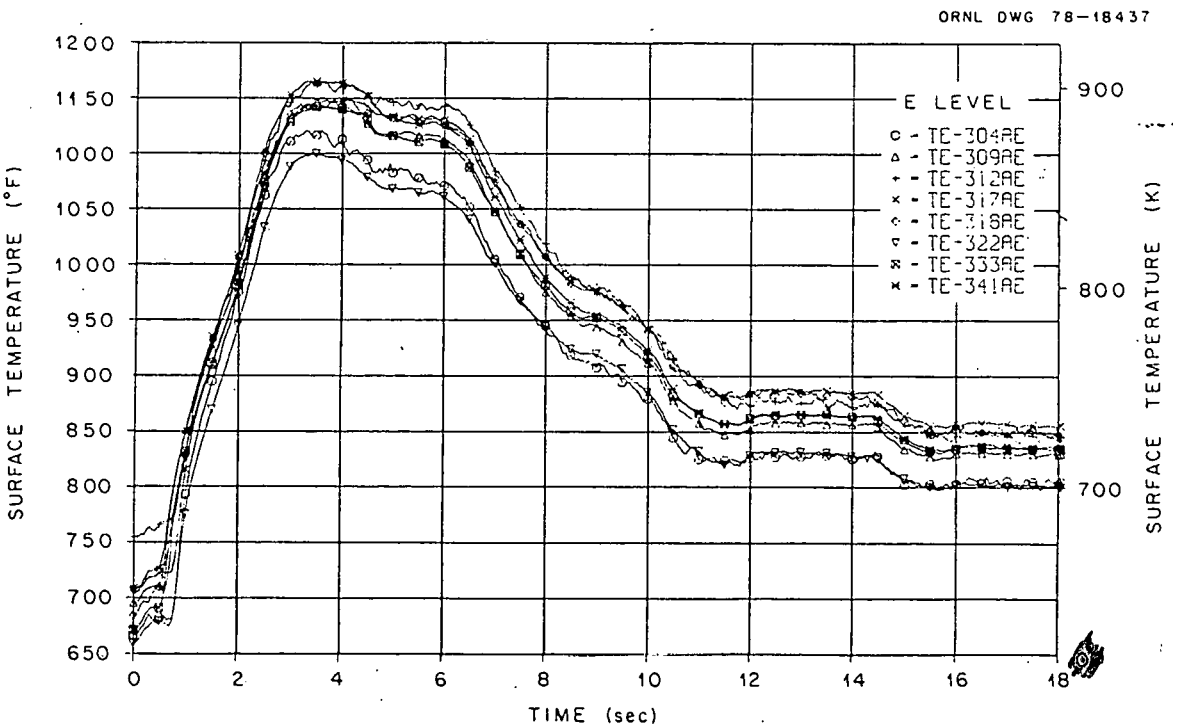

Fig. 8.5 ORINC calculated FRS surface temperatures, level E, THTF test 105, case 2.

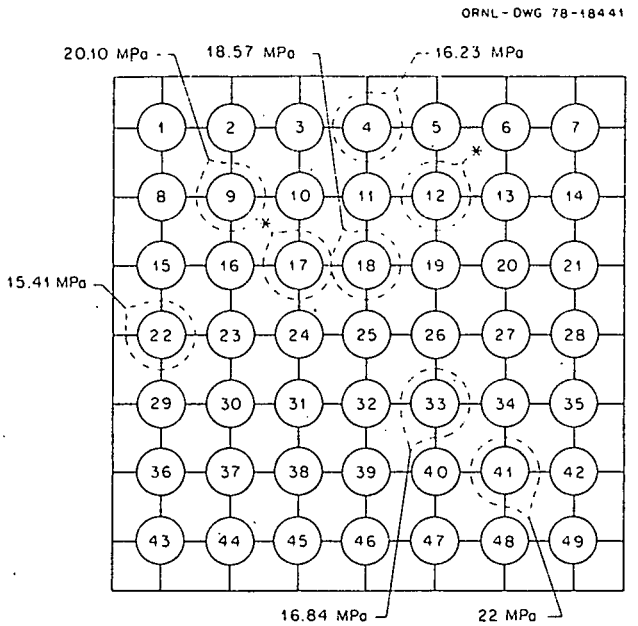

Fig. 9.7 Distribution of steady-state pressure predicted using case 2 (superimposed on cross section of bundle 1 core at level E for test 105).

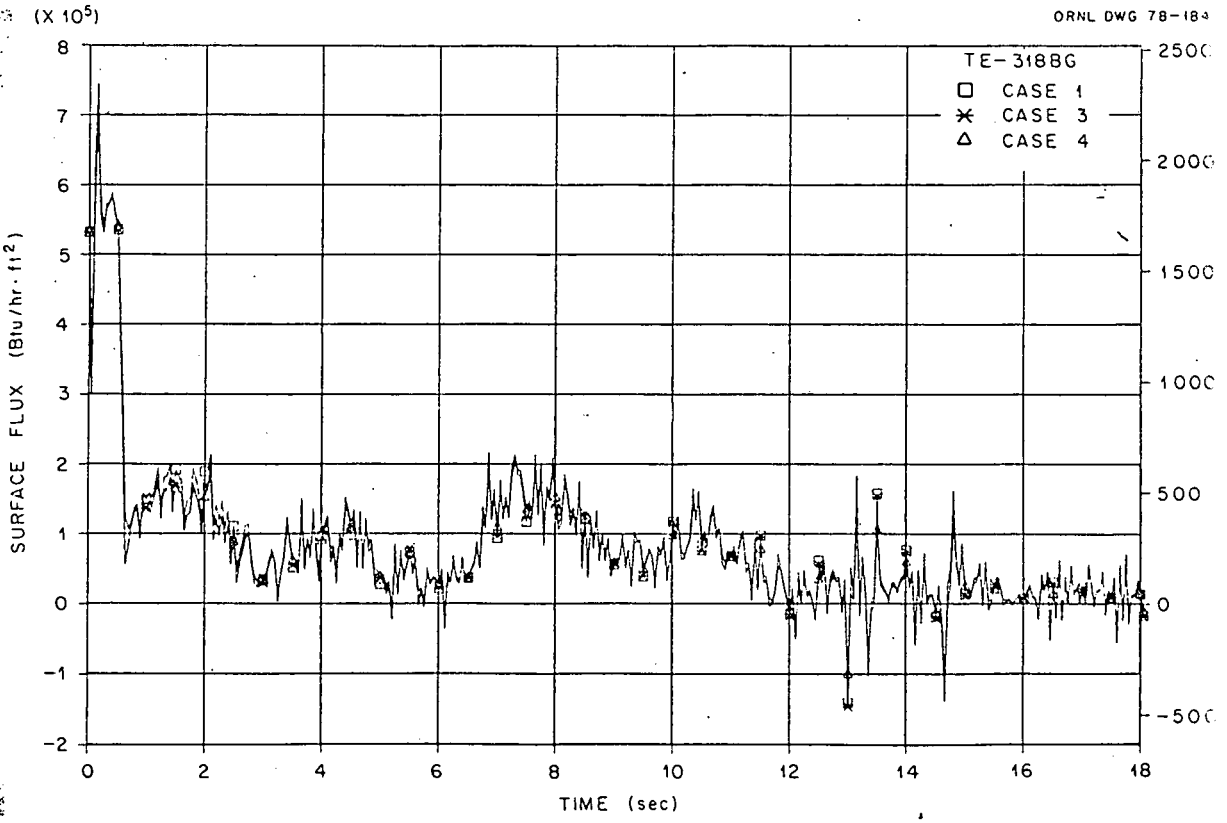

Fig. 10.8 ORINC calculated FRS surface heat flux for cases 1, 3, and 4 (TE-318BG, THTF test 105, 0 to 18 s).

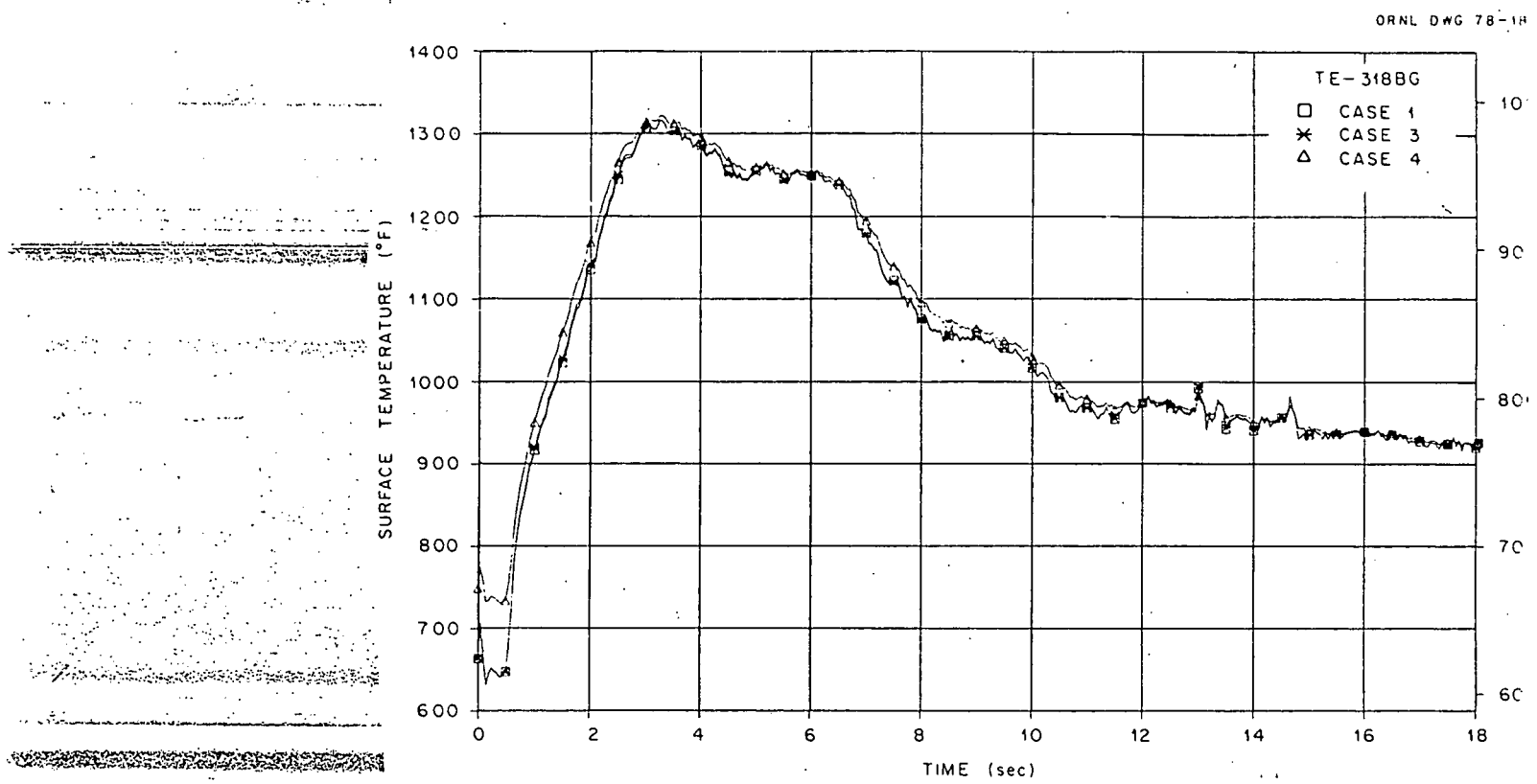

Fig. 11.9 ORINC calculated FRS surface temperatures for cases 1, 3, and 4 (TE-318BG, THTF test 105, 0 to 18 s).

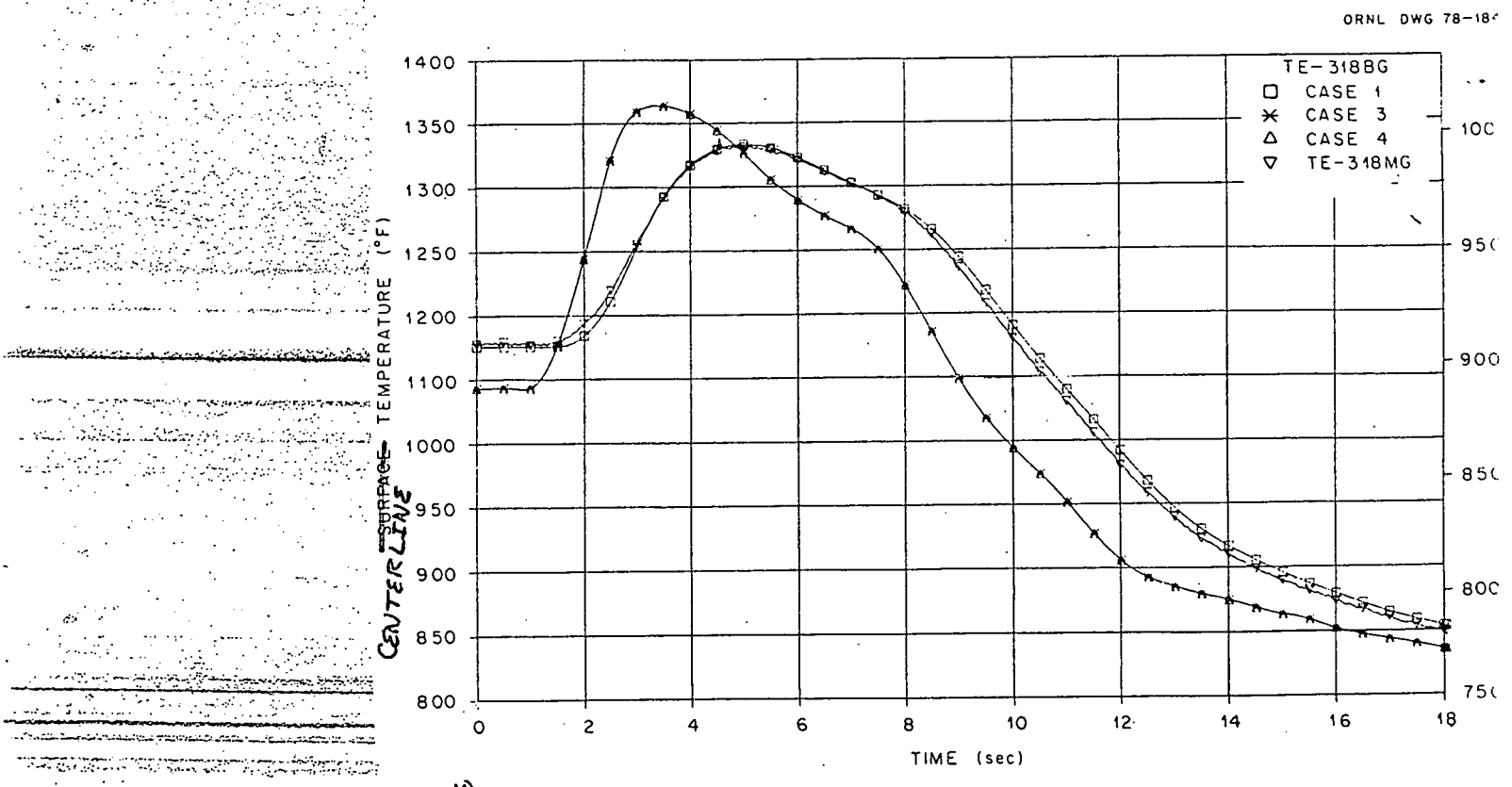

Fig. 12.10 ORINC calculated FRS centerline temperature for cases 1, 3, and 4 (TE-318BG, THTF test 105, 0 to 18 s).

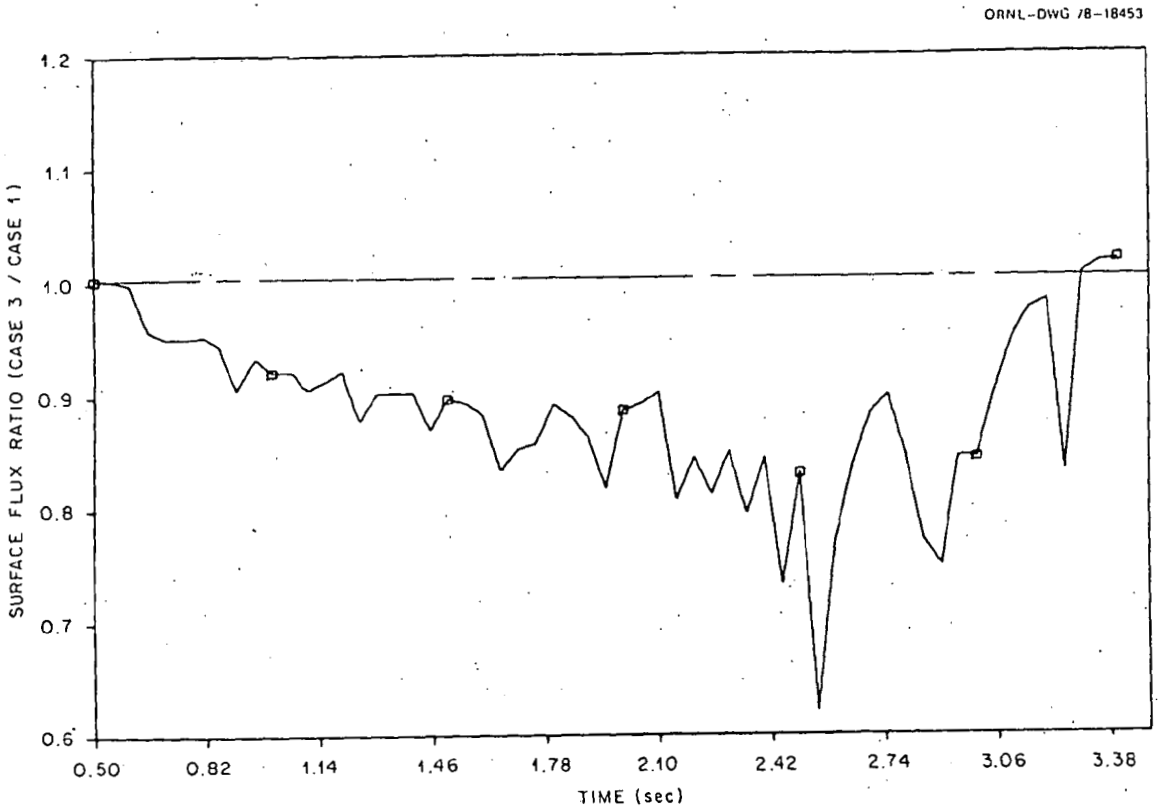

Fig. 13. 11 Ratio of surface heat fluxes for cases 1 and 3 from 0.5 to 3.4 s.